Thermo-Oxidative Decomposition Kinetics of Elastomeric Composites Based on Styrene-(ethylene-butylene)-Styrene Triblock Copolymer and Organomontmorillonite

Sunan Saikrasun,[1] Taweechai Amornsakchai[2]

[1]*Materials Science Research Unit, Department of Chemistry and Center of Excellence for Innovation in Chemistry, Faculty of Science, Mahasarakham University, Mahasarakham 44150, Thailand*
[2]*Center for Alternative Energy, Department of Chemistry and Center of Excellence for Innovation in Chemistry, Faculty of Science, Mahidol University, Bangkok 10400, Thailand*

Received 6 October 2009; accepted 3 October 2010
DOI 10.1002/app.33516
Published online 11 February 2011 in Wiley Online Library (wileyonlinelibrary.com).

ABSTRACT: The elastomeric nanocomposites based on organomontmorillonite (OMMT) and styrene-(ethylene-butylene)-styrene (SEBS) thermoplastic elastomer were prepared by melt processing using maleic anhydride grafted SEBS (SEBS-*g*-MA) as compatibilizer. Thermo-oxidative decomposition behavior of the neat components and the nanocomposites were investigated using thermogravimertic analysis (TGA) in air atmosphere. The isoconversional method is employed to study the kinetics of thermo-oxidative degradation. The heating modes and the composition of nanocomposites were found to affect the kinetic parameters (E_a, ln$A$ and n). The E_a and ln$A$ values of SEBS, OMMT, and their composites are much higher under dynamic heating than under isothermal heating. The reaction order (n) of OMMT was lower than those of SEBS and their composites. The obtained TG profiles and calculated kinetic parameters indicated that the incorporation of OMMT into SEBS significantly improved the thermal stability both under dynamic heating and under isothermal heating. The simultaneously obtained DSC data showed that the enthalpy of thermal decomposition decreased with OMMT loading. No significant change in the nonisothermal and isothermal stability of the nanocomposites with addition of SEBS-*g*-MA. © 2011 Wiley Periodicals, Inc. J Appl Polym Sci 120: 3337–3349, 2011

Key words: clay; nanocomposite; styrene-(ethylene-butylene)-styrene (SEBS); thermal degradation; decomposition kinetics

INTRODUCTION

Scientific research on preparation and characterization of polymer/clay nanocomposites has grown continuously in the 21st century with the general aim of developing new materials with improved properties. Montmorillonite (MMT) is a layered, mica-type clay mineral widely used in nanocomposite preparation.[1] Its layer structure consists of two silica tetrahedral sheets and an edge-shared octahedral sheet of either aluminum or magnesium hydroxide. Staking layers ~ 1-nm thick with a weak dipolar force leads to interlayers or galleries between layers. The galleries are normally occupied by cations such as Na^+, Ca^{2+}, Mg^{2+}, with which it is easy to form organomontmorillonite (OMMT) by an alkylammonium ion-exchange reaction. OMMT can be either intercalated by macromolecules or exfoliate when they are dispersed in polymer. The clay-containing nanocomposites have attracted great interest to both academic and industrial researcher due to their ability to display synergistically advanced characteristics with small amount of clay loading (e.g., 3 wt %). The typical improved properties include barrier properties, flame retardancy, thermal stability chemical and dimensional stability and mechanical properties when compared to their micro- and macrocomposites counterparts and their neat polymer matrices.[2–4] Since then, the outstanding material properties have led to profound research on the creation of polymer/clay nanocomposites in which the polymer matrix included polyolefins,[5–10] polyolefin rubbers,[11–13] polyamides,[14–16] polyesters,[17–19] etc. Moreover, some attention has been paid so far to the development of thermoplastic elastomers (TPEs).[2,3,20–23]

Styrene-(ethylene butylene)-styrene (SEBS) triblock copolymer is a commercially important TPE used in various applications, such as adhesives, sealants, coatings, footwear, automotive parts, impact modifier in engineering plastics, wire insulations, etc.,

Correspondence to: S. Saikrasun (sunan.s@msu.ac.th).
Contract grant sponsor: Center of Excellence for Innovation in Chemistry (PERCH-CIC), Commission on Higher Education, Ministry of Education.

because of its good balance of mechanical properties along with favorable processability and recyclability.[24] However, to address the demands of engineering applications in more severe environmental conditions, enhancement of the performance properties of the copolymer is required. To improve its properties, the incorporation of the aforementioned intercalated clay into SEBS has been reported in some studies.[2,20–23] Most studies have been explored the high potential of clay as a minor nanofiller component by improving the physical properties of the nanocomposites.

Normally, the polymer must encounter elevated temperature at almost every stage in manufacturing, compounding, and processing stages in service and during repairing step. Therefore the understanding of thermal degradation behavior of individual polymer and their composites is very important in predicting their suitability in the specific filed of applications. Thermogravimetric analysis (TGA) is a simple technique widely used to characterize the thermal decomposition of polymeric materials. The TGA data can also be used in studying the kinetics of thermal decomposition, which provide an insight into the thermal stability of polymers. Although a number of studies dealt with the preparation and characterization of polymer nanocomposites, few attempts have been made to analyze the thermal decomposition kinetics of polymer nanocomposites.[25,26] Marazzato et al.[25] studied the nonisothermal degradation of nanocomposites based on functionalized polyethylenes. They found that in the presence of clay, the thermal stability in nitrogen atmosphere decreases, while the thermal stability in air increases. They also found that the effect of clay on the degradation behavior of the polymer matrix is more pronounced for the nanocomposites possessing fully exfoliated structure than that of the nanocomposites containing intercalated clay stacks. Moreover, the thermal degradation kinetics of polypropylene/clay microcomposites and nanocomposites were investigated by Qin et al.[26] They concluded that the reaction order for the degradation of PP/clay composites altered from first-order to zero-order which is associated with the acidic sites (H^+) created on the clay layers. They also found that the activation energy increases as the clay particles in the PP matrix become smaller and exfoliated. However, to the authors' best knowledge, the kinetic analysis of thermal decomposition for clay/SEBS elastomeric nanocomposites has not been systematically studied. In this work, we attempt to clarify the thermal decomposition behavior and quantitatively elucidate the thermal stability of the elastomeric nanocomposites by using kinetic analysis close to real processing and application atmosphere.

EXPERIMENTAL

Materials

Styrene-ethylene butylene-styrene (SEBS) triblock copolymer, Kraton G1650, with a styrene/rubber wt % ratio of 29/71 was purchased from Toyota Tsusho (Thailand). The specific gravity of SEBS is 0.91. Organoclay which is commercially available under the trade name "Claytone® HY" produced by Southern Clay Products, USA, was purchased from local distributor and used as received. According to product literature, the organic modifier is bis(hydrogenated tallow alkyl) dimethyl ammonium. This particular grade was chosen for this study as it is recommended for low polarity systems and does not require activator. The compatibilizer, maleic anhydride-grafted-SEBS (SEBS-*g*-MA) produced by Sigma-Aldrich®, USA, was purchased from S.M. Chemicals Supplies, Thailand. From the Sigma-Aldrich® product literature, the compatibilizer contains $\sim$ 2 wt % maleic anhydride and has a melt flow rate of 22 g/10 min.

Preparation of the composites

The SEBS/OMMT composites at various compositions of OMMT and SEBS-*g*-MA were prepared by melt blending in an internal mixer [Haake Rheomex, Thermo Electron (Karlsruhe) GmbH, Karlsruhe, Germany] at a temperature of 165°C and a rotor speed of 100 rpm for 10 min. The composites were then compression-molded into a sheet about 1-mm thick. The molding condition was 180°C under a pressure of 20 tons for 10 min. The sample codes of the elastomeric composites are designated as SEBS-*X* where *X* depicts the content of OMMT in phr. For the compatibilized composites, the sample codes are designated as SEBS-*X*/*Y*MA where *X* and *Y* depict the contents of OMMT and SEBS-*g*-MA in phr and wt %, respectively.

FT-IR characterization

For FT-IR analysis, the samples were thermally compressed as a thin film using the same condition as that of the sheet preparation. The infrared spectra of the thin film samples were recorded on a FT-IR Spectrophotometer (Perkin–Elmer, Spectrum GX, UK) at resolution of 4 cm^{-1} for 32 scans from 4000 to 400 cm^{-1}.

Morphological characterization

The fracture surface of the composites with and without compatibilizer were observed under the scanning electron microscope (SEM) (LEO 01455VP, Cambridge, England) operated with the voltage of 20 kV. Prior to examination, the composite samples

were immersed in liquid nitrogen for 30 min and then fractured. The specimens were sputter-coated with gold for enhanced surface conductivity.

X-ray diffraction measurement

X-ray diffraction (XRD) equipment (Bruker AXS D8, Karlsruhe, Germany) with a generator voltage of 40 kV and a generator current of 40 mA was employed to evaluate the dispersion of OMMT in the composites. The X-ray source was Cu Kα radiation at a wavelength of 0.154 nm. The difractograms were scanned in the 2θ range from 1.5° to 10° at a rate of 0.02° s^{-1}.

Thermal decomposition analysis by simultaneous TG and DSC measurements

Thermogravimetric analysis (TGA) was carried out using TA instruments, SDT Q600 (Luken's drive, New Castle, DE). The neat and composite samples of 8–10 mg were loaded in alumina crucible and then nonisothermally heated from ambient temperature to 1000°C at five different heating rates as 5, 10, 15, and 20°C min^{-1}. The TGA was performed in air with the flow rate of 100 mL min^{-1}. The TG and DSC data were simultaneously recorded online in TA instrument's Q series explorer software. The analyses of simultaneous TG and DSC data were done using TA Instrument's Universal Analysis 2000 software (version 3.3B).

The isothermal tests were measured at 300, 320, 340, and 360°C for 100 min. Before isothermal heating, the sample was heated at a rate of 20°C min^{-1} from ambient temperature to the selected temperature of isothermal degradation. As soon as the system reached the selected temperature, the variations of sample weights with times were registered. The isothermal tests were performed in air with the flow rate of 100 mL min^{-1}. The analyses of isothermal TG data were carried out using the same software as those of the dynamic TG data.

Kinetic analysis of nonisothermal decomposition

To obtain the reliable kinetic information on thermal and thermo-oxidative degradation, the isoconversional (model-free) method that allows for evaluating kinetic parameters without choosing the reaction model was applied. Flynn-Wall-Ozawa (F-W-O) method[27,28] is a relatively simple method of determining activation energy directly from weight loss versus temperature data, obtained at several heating rates. This method is shown by the following equation:

$$\ln \beta = \left[\frac{AE_a}{Rg(\alpha)}\right] - 5.3305 - 1.0516\frac{E_a}{RT} \quad (1)$$

where β is a heating rate in °C min^{-1}, E_a is an apparent activation energy (kJ mol^{-1}), A is a pre-exponential factor, R is an universal gas constant (J K^{-1} mol^{-1}), T is an absolute temperature (K) and $g(\alpha)$ is an integral reaction type of kinetic function.

The Kissinger method[29] is widely used to calculate the kinetic parameters at a fixed conversion. This method involves the temperature (T_{max}) at the maximum weight-loss rate $(d\alpha/dt)_{max}$. The apparent activation energy can be determined by using this method without precise knowledge of the reaction mechanism. This method is based on the following equation:

$$\frac{E_a\beta}{RT_{max}^2} = An(1-\alpha_{max})^{n-1}e^{-E_a/RT_{max}} \quad (2)$$

Kissinger assumes that the product $n(1-\alpha_{max})^{n-1}$ is independent of β and the following expression can be derived:

$$\ln\left(\frac{\beta}{T_{max}^2}\right) = \ln\left[n(1-\alpha_{max})^{n-1}\left(\frac{AR}{E_a}\right)\right] - \frac{E_a}{RT_{max}} \quad (3)$$

The slope of $\ln(\beta/T_{max}^2)$ versus $1/T_{max}$ equals to $-E_a/R$, whereas its intercept (I) equals to $\ln\left[n(1-\alpha_{max})^{n-1}(AR/E_a)\right]$. The n-value can be estimated from the following equation:

$$n = \left[(1-\alpha_{max})\,E_a\,e^I\right]\frac{e^{-\frac{E_a}{RT_{max}}}}{R(d\alpha/dt)_{max}} \quad (4)$$

Then, the A value can be calculated by the substituting n into the intercept equation:

$$I = \ln\left[n(1-\alpha_{max})^{n-1}\left(\frac{AR}{E_a}\right)\right] \quad (5)$$

Kinetic analysis of isothermal decomposition

Generally, the rate of solid state degradation reaction ($d\alpha/dt$) can be described by[30–32]

$$\frac{d\alpha}{dt} = k(T)\,f(\alpha) \quad (6)$$

In eq. (2), $k(T)$ represents the reaction rate constant and $f(\alpha)$ is a conversion function. By substitution of the Arrhenius equation, $k(T) = Ae^{-E_a/RT}$, eq. (2) becomes

$$\frac{d\alpha}{dt} = f(\alpha)Ae^{-E_a/RT} \quad (7)$$

By integration of eq. (7), the integral type of kinetic function, $g(\alpha)$, is obtained:

$$g(\alpha) = Ae^{-E_a/RT}t \quad (8)$$

where t is a degradation time. Depending on the assumed reaction mechanism, many expressions for $g(\alpha)$ were derived.[32–34] Kinetic parameters can be obtained from isothermal kinetic data by applying these rate laws with traditional model-fitting methods or with isoconversional (model-free) methods. By taking the natural logarithm of eq. (4), the isoconversional equation is derived:

$$\ln t = \ln g(\alpha) - \ln A + \frac{E_a}{RT} \quad (9)$$

Equation (9) is called standard isoconversional method.[35] The natural logarithm of time t corresponding to a certain weight loss α is linearly dependent on the reciprocal of temperature T. Provided that the order of decomposition reaction n keeps constant within the temperature and weight loss interval under consideration, E_a and $\ln A$ can be respectively, calculated in terms of the slope and intercept of the linear relationship of $\ln t$ versus $1/T$ for various α values.

RESULTS AND DISCUSSION

FT-IR characterization of compatibility effect

The FTIR spectra of SEBS, SEBS-*g*-MA, and SEBS/OMMT composites containing various compatibilizer contents are depicted in Figure 1. With the presence of OMMT, Figure 1(A), the absorption bands at 1043 and 3631 cm^{-1} correspond to the asymmetric Si—O—Si and —OH stretching of silicates within the composite system.[3] To clearly elucidate the compatibilizer dosage effect, the expanded region of FTIR spectra is shown in Figure 1(B). For SEBS, the absorption bands for the aromatic overtones are found at 1735, 1803, 1871 cm^{-1}. As the OMMT was incorporated, the above typical absorption region of the aromatic overtone at 1735 cm^{-1} shifted to 1721 cm^{-1} suggesting that OMMT preferably interacted with polystyrene (PS) block in SEBS, due to the slight Lewis base character imparted by the phenyl ring in the PS block.[36] As the 2.5 and 5 wt % SEBS-*g*-MA was incorporated, no significant change of the typical absorption band is observed. No much effect was found on the enhanced interaction between the maleic anhydride group on SEBS and hydroxide group on the OMMT. Perhaps the overlapping aromatic overtone signals on PS blocks with the carbonyl group on maleic anhydride resulted in an insignificant maleated compatibilizer contribution.[3,37]

SEM studies

SEM images of the composites are very informative with respect to their fracture surface morphology and the distribution of clay in the polymer matrix.

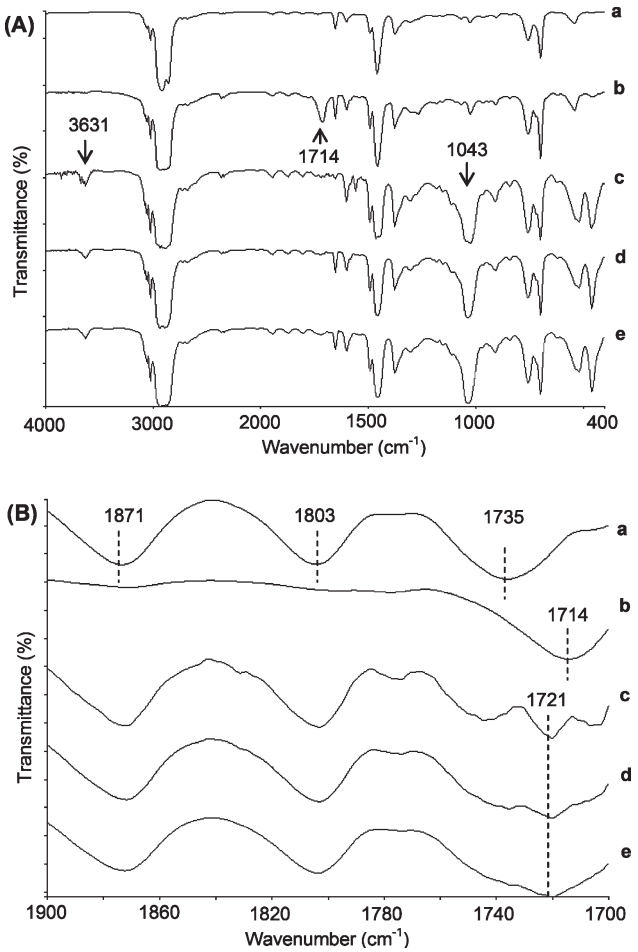

Figure 1 FTIR spectra (A) and expanded region from 1700 to 1900 cm^{-1} (B) of (a) SEBS, (b) SEBS-*g*-MA, (c) SEBS-5, (d) SEBS-5/2.5MA, and (e) SEBS-5/5MA.

Such observation on fracture surfaces SEBS-5, SEBS-5/2.5MA, and SEBS-5/5MA are presented in Figures 2(a–c), respectively. In the absence of compatibilizer, a split of the polymer surface is clearly observed, whereas more smooth surface with less splitting area are observed on the fracture surface of the compatibilized composites as seen from Figures 2(b,c). The morphological results for the compatibilized composites indicate that the presence of OMMT and compatibilizer improves the connectivity of the matrix phase. However, due to the limited resolution of SEM, the layered aggregates of OMMT resulting from the intercalation which was normally dispersed at a regular interval across the thickness of the polymer sheet and the crack pass through along the edges of the aggregates are not observed.

Dispersion of OMMT in the composites

XRD is a useful technique for characterization of clay and polymer/clay composites. This technique allows the precise measurement of silicate layer spacing and the dispersion of OMMT in the polymer

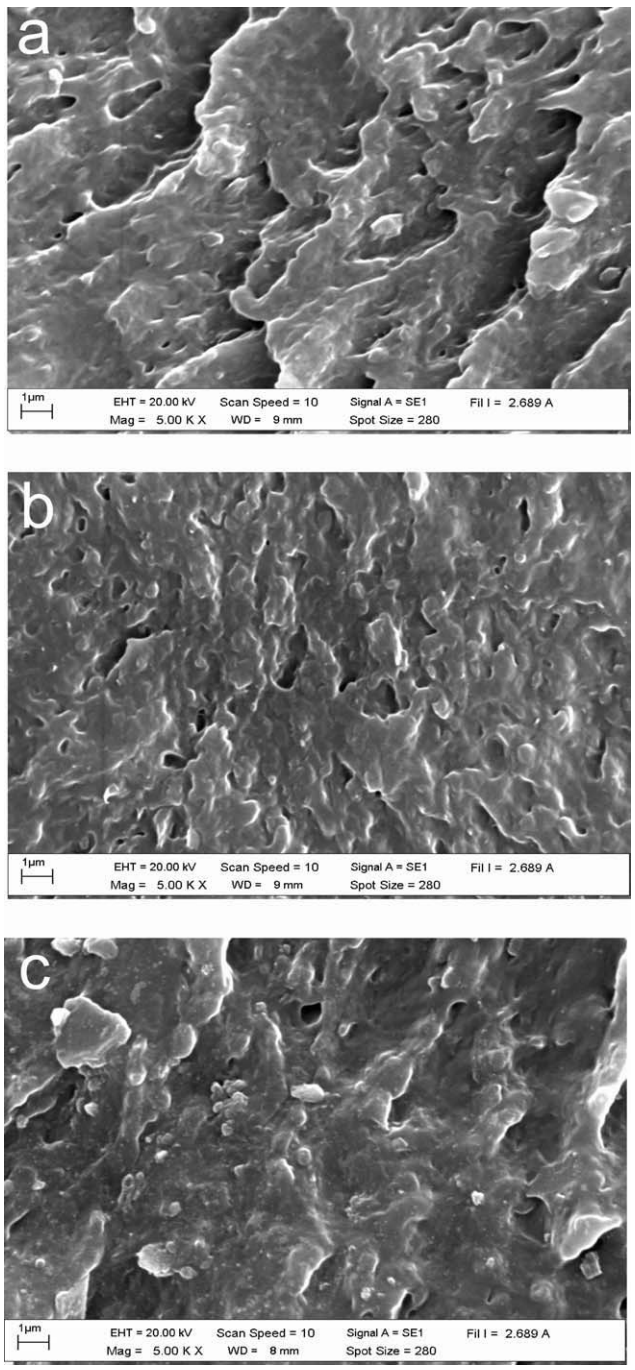

Figure 2 SEM micrographs of fracture surface for (a) SEBS-5, (b) SEBS-5/2.5MA and (c) SEBS-5/2.5MA.

matrix. Figure 3 shows the XRD patterns of SEBS, OMMT, SEBS-5, SEBS-5/2.5MA, and SEBS-5/5MA. The XRD spectra of OMMT possesses three characteristic reflection peaks at 2θ value = 2.5, 4.3, and 7.2 corresponding to *d*-spacing of 3.4, 2.1 and 1.27 nm, respectively. The shift of the sharp d_{001}-plane spacing peak of OMMT from 2θ value = 2.5 to the lower diffraction angle in the compatibilized composites containing 5 wt % (SEBS-5/5MA) is clearly observed, indicating that SEBS has been able to intercalate into gallery spaces of the organoclay in the presence of the optimum compatibilizer content. However, no significant change occurs in the absence or relatively low content of SEBS-*g*-MA.

Thermal decomposition behavior of SEBS/OMMT composites under dynamic heating

The effect of OMMT contents on nonisothermal decomposition behavior and the corresponding simultaneous DSC curves of the SEBS/OMMT composites in air are presented in Figures 4(A,B), respectively. The thermal degradation of SEBS and OMMT occur in at least two steps. The neat SEBS exhibits the first major weight-loss in the range of 250–380°C, whereas the first major weight-loss of the OMMT appears in the range of 200–350°C. For the thermal degradation of SEBS, the chain degradation, scission, and oxidation which occur primarily at the boundary of styrene-olefin phase, giving rise to the formation of acetone end groups on the styrene units and carboxylic acids on the olefin chain ends.[38] For OMMT, the first major step of weight-loss corresponds to the decomposition of organic components. The content of the organic substance is about 30 wt %. Interestingly, the significant improvement of thermal stability of SEBS is clearly observed with OMMT loadings as seen from the remarkable shift of TG curves to high temperature. The significant improvement in thermal stability of the OMMT-containing composites may be due to the accumulation and reassembly of silicate layer on the surface of burning material, offering a great barrier effect to hinder the formation of small molecules, resulting from thermal decomposition and simultaneous resisting their movement during desorption from the surface.[39]

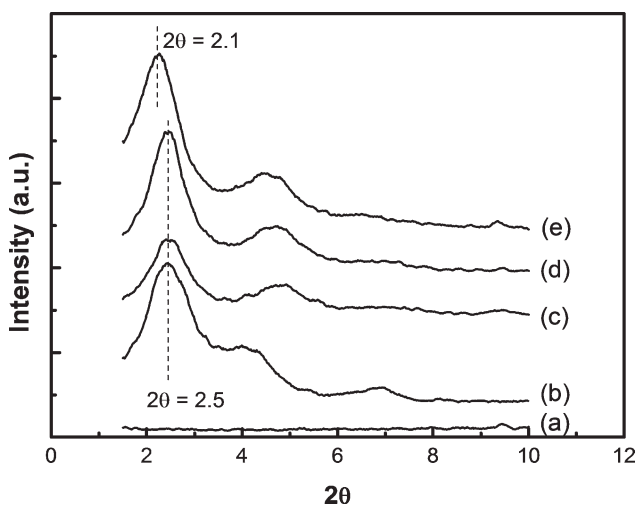

Figure 3 XRD patterns of (a) SEBS, (b) OMMT, (c) SEBS-5, (d) SEBS-5/2.5MA, and (e) SEBS-5/5MA.

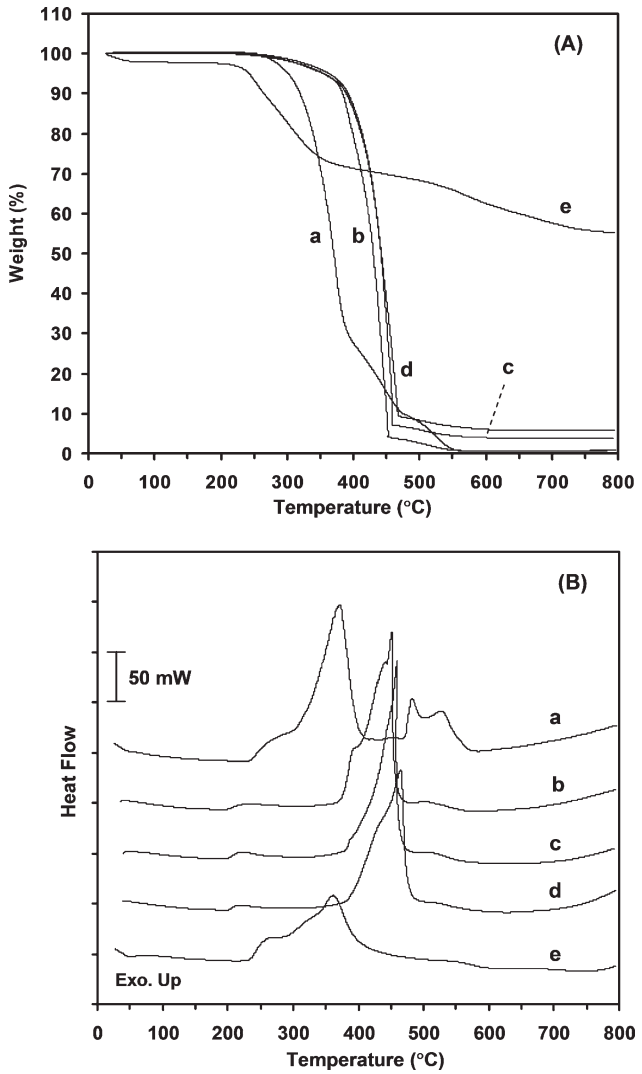

Figure 4 Dynamic TG (A) and corresponding simultaneous DSC (B) curves of SEBS/MMT nanocomposites containing various blend compositions: (a) SEBS, (b) SEBS-2, (c) SEBS-5, (d) SEBS-10, and (e) OMMT.

To clearly elucidate the OMMT-dosage dependence of thermal stability in more quantitative way, the thermal characteristics of the major weight-loss step of all samples in air, are compared and summarized in Table I. T_{onset} represents the onset degradation temperature. T_{max} represents the temperature at the maximum weight-loss rate, $(d\alpha/dt)_{max}$. Although the low values of T_{onset} and T_{max} of OMMT is observed and the relatively small amount of OMMT is incorporated into the SEBS, it is seen that T_{onset} of the nanocomposites are much higher than those of both the polymer matrix and OMMT. This result reveals the high potential of OMMT as an enhancing thermal stability material in the composite system. It is seen that $(d\alpha/dt)_{max}$ of the nanocomposites are much higher than those of SEBS and OMMT and seems to progressively increase with OMMT loading. Moreover, the amount of char residues progressively increases with increasing the content of OMMT.

The simultaneous DSC traces of thermal degradation for the SEBS, OMMT and the nanocomposites containing various OMMT contents in air are shown in Figure 4(B). The corresponding peak temperature (T_d) and enthalpy (ΔH_d) associated with the thermal degradation process is also presented in Table I. The exothermic degradation process is observed for all the samples due to the fact that the concurrent and further degradation mechanisms in air tend to involve the formation reaction. SEBS shows a very broad degradation exotherm that stretches from 230 to 560°C with a peak maximum (T_d) at 372°C, whereas the OMMT exhibits a broad degradation exotherm with a peak maximum at 362°C. By comparing with the neat SEBS and OMMT at the same heating rate and atmosphere as the controlling factors, the exothermic peaks of the SEBS/OMMT nanocomposites shift to higher temperature similar to the T_{onset} and T_{max} gained from the TG profiles. Note that the enthalpy of thermal decomposition decreases with OMMT loading.

Effect of compatibility on thermal decomposition behavior

Figure 5(A,B) show the dynamic TG curves and the corresponding simultaneous DSC curves, respectively, of the SEBS-5/2.5MA and SEBS-5/5MA compared to those of the uncompatibilized SEBS-5. The

TABLE I
Thermo-Oxidative Decomposition Characteristics for the First Major Weight Loss Stage of SEBS/OMMT Nanocomposites

Sample	T_{onset} (°C)	T_{max} (°C)	$(d\alpha/dt)_{max}$ (wt % min^{-1})	Char yield at 600°C (wt %)	T_d (°C)	ΔH_d (kJ g^{-1})
SEBS	333	367	12.6	0.30	372	7.87
SEBS-2	407	448	27.8	0.60	451	5.33
SEBS-5	421	456	35.1	3.98	460	4.74
SEBS-10	410	459	34.9	6.01	465	4.44
OMMT	232	252	2.50	62.2	362	4.24
SEBS-5/2.5MA	412	461	34.3	3.27	464	4.88
SEBS-5/5MA	419	461	30.2	2.76	463	4.59

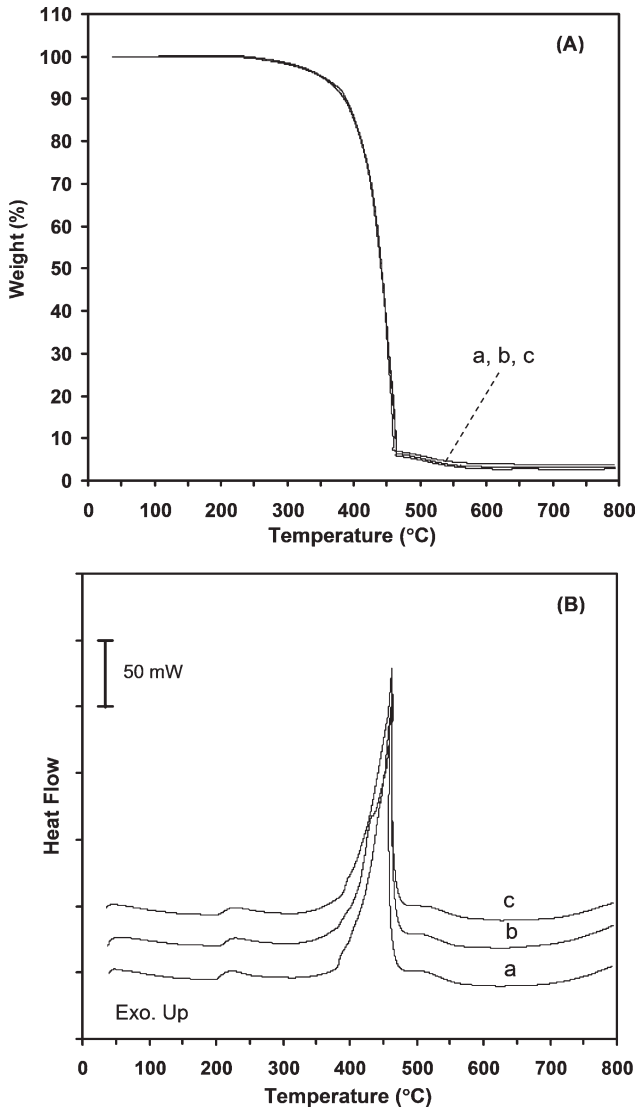

Figure 5 Dynamic TG curves (A) and corresponding simultaneous DSC curves (B) of compatibilized SEBS/OMMT nanocomposites: (a) SEBS-5, (b) SEBS-5/2.5MA, (c) SEBS-5/5MA.

TG profiles for all samples show a single weight-loss step at 250–470°C. As seen from the TG curves, no significant change in thermal stability among SEBS-5 and both of the compatibilized nanocomposites are observed. This result is similar to those of the compatibilized liquid crystalline polymer/polypropylene microcomposite and compatibilized SEBS/clay (Cloisite) nanocomposite studied by one of us[40] and Chang et al.,[21] respectively. That is, the presence of SEBS-*g*-MA slightly affects the TG profiles of the composite systems. In general, the improvement of mechanical properties of the polymer composites can mostly be achieved by enhancing the compatibilization between the interfaces of the mixture components. In the present study, in terms of thermal stability, the role of compatibized phenomena seems to little affect the TG profile of the composites. Marazzato et al.[25] studied the kinetics of nonisothermal degradation of nanocomposites based on functionalized polyethylenes. They reported that the effect of clay on improving the thermal stability under heating in air is more pronounced for the nanocomposites having better dispersion of clay layers, leading to a better barrier effect for the oxygen flow. For the typical behavior of clay/polymer system during combustion, heat transfer from external source promotes thermal decomposition of clay and polymer. It should be noted that, for the investigated composite samples, the amount of residue almost corresponds to the inorganic content of OMMT in the sample. This results in the accumulation and reassembling of clay platelets on the surface of burning material. The inorganic residue acts as the insulator and mass transport barrier that enhance the thermal stability by slowing the oxygen flow and the volatile product generated during decomposition.[39] In this study, the thermal stability of the compatibilized composite, compared with that of the uncompatibilized are comparable as seen from the overlapping of TG curves in Figure 5(A). This may be due to that the presence of the compatibilizer does not significantly improve the dispersion of clay. However, the improvement of thermal stability is not only contributed from the inherent properties of clay and its dispersion but also the inherent nature of polymer matrix used in the composite system.

Nonisothermal kinetic analysis

Isoconversional method is one of nonisothermal multiplescan techniques for studying kinetics. This method is also called model-free method because no kinetic model was set before the calculation. It appears that the analytic techniques based on several curves obtained at different heating rates present a lower risk of creating errors than do techniques based on a single thermogram. To understand the decomposition kinetics of the neat components and the composites in easier way, the analytical techniques were unified by using isoconversional methods (Flynn-Wall-Ozawa and Kissinger).[27–29] These techniques allow for evaluating reliable kinetic parameters without having to know the reaction model. In this study, the kinetic analysis of SEBS, SEBS-5, and OMMT was investigated. However, the kinetics of thermal decomposition for the compatibilized composite was not studied here since there is no significant difference in TG profiles of the compatibilized- and uncompatibilized composites. The nonisothermal TG curves of SEBS, SEBS-5, and OMMT at four different heating rates of 5, 10, 15, and 20°C min^{-1} in air are shown in Figure 6. The TG curves reveal the different profiles depending on heating

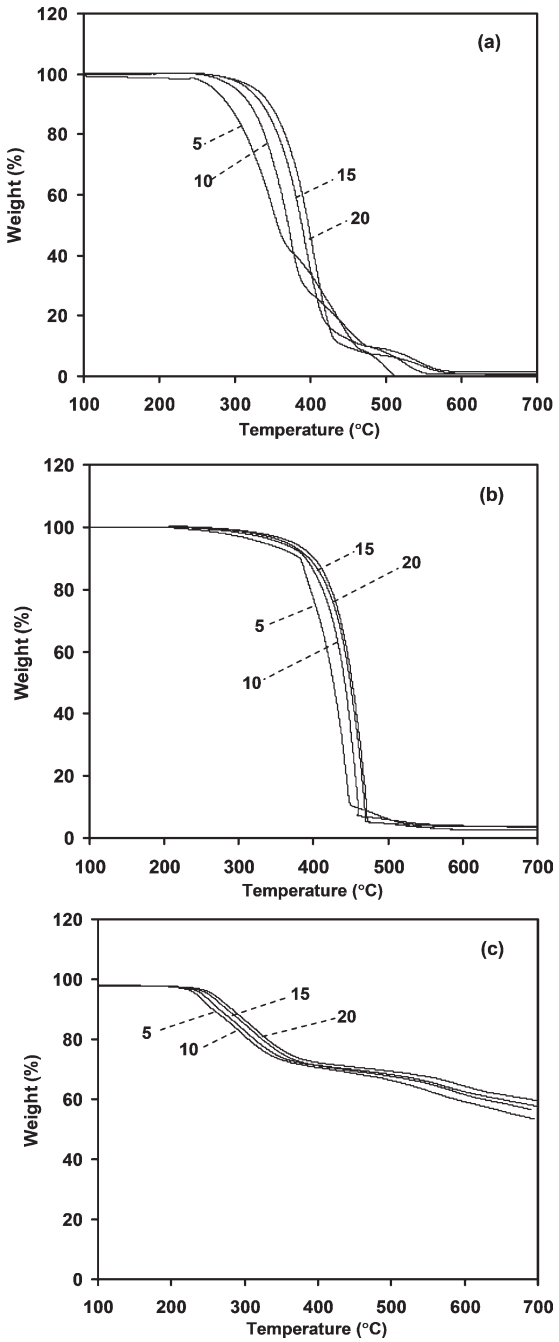

Figure 6 Dynamic TG curves of SEBS (a), SEBS-5 (b), and OMMT (c) at heating rates of 5, 10, 15, and 20°C min^{-1} in air.

rate and the composition. It is seen that the TG curves progressively shift to the higher temperature as the heating rate increases. Generally, at low heating rate, the sample temperature is more uniform and diffusion of gaseous products could occur within the sample, thus lowering the decomposition temperature. In the same meaning, the shift of the TG curves to the higher temperature with increasing heating rate could be attributed to the short time required for a sample to reach a given temperature at high heating rate.[41]

In general, thermal degradation of polymers usually involves multiple steps that are most likely to have different mechanism and activation energies. The relative contribution of these steps to the overall degradation rate changes with both temperature and extent of reaction. This means that the effective activation energies determined from thermal analysis data alone are not capable of revealing this type of reaction complexity. Therefore, to avoid the need to know decomposition mechanism required for some model fitting, we use a model-free approach to kinetic analysis in this study. This approach rests upon the isoconversional method whose application to thermal degradation of polymers often yields an activation energy, which varies with the extent of conversion. Knowledge of the dependence activation energy on conversion extent assists in both detecting multi-step process and drawing certain mechanistic conclusion. Moreover, it is sufficient to predict the reaction kinetics over a wide temperature region and the isoconversional method yield similar (but not identical) dependence of the activation energy on the extent of conversion. In this study, the activation energy calculated by F-W-O and Kissinger methods is called apparent activation energy because it is the sum value of activation energies of the chemical reactions and physical processes in thermal degradation. The plots of isoconversional activation energy as a function of conversion extent (α) using F-W-O method for SEBS, SEBS-5 and OMMT are shown in Figure 7. The activation energy of SEBS gradually increases from 68.5 to 159 kJ mol^{-1} as α increases from 0.1 to 0.9. This should be ascribed to the nature of chain degradation, scission, and oxidation which

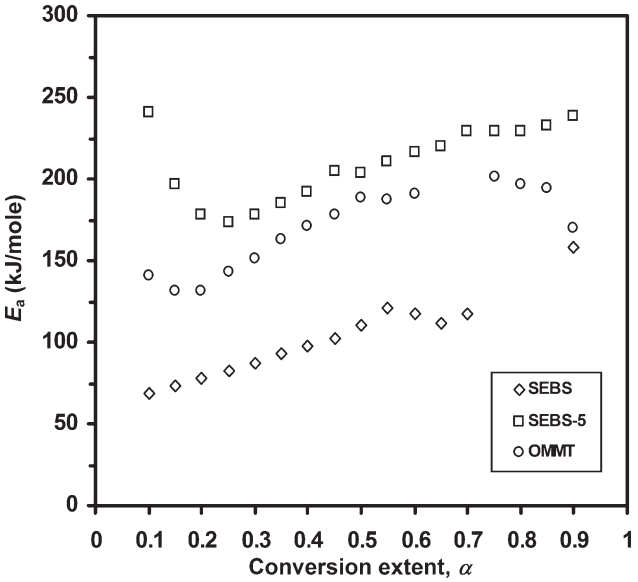

Figure 7 Dependence of activation energy (E_a) on conversion extent (α) for thermal degradation of SEBS, SEBS-5, and OMMT in air.

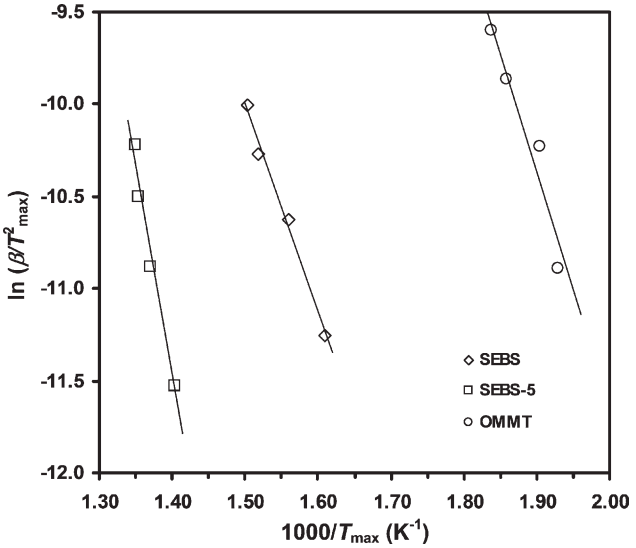

Figure 8 The Kissinger plots for the first stage degradation of SEBS, SEBS-5, and OMMT in air.

occur primarily at the boundary of styrene-olefin phase as suggested by Allen et al.[38] The slight increase in activation energy with increasing α revealed in this study is similar to those of commercial polyolefins such as PP and PE.[42] The activation energy of SEBS-5 and OMMT drops at low α range (α = 0.1-0.2) and then increases from ≈ 174 to ≈ 240 kJ mol^{-1} for SEBS-5 and ≈ 130 to ≈ 195 kJ mol^{-1} for OMMT in the entire range of α. The variation in activation energy with the extent of reaction for all samples indicates that multi-step reaction mechanism occurs during thermo-oxidative degradation. It is seen that the activation energy of OMMT is much higher than that of SEBS throughout the range of α. For instance, the activation energy of OMMT is ≈ 90 kJ mol^{-1} higher than that of SEBS at α = 0.5. Interestingly, although the OMMT shows much higher value of activation energy when compared with SEBS, the incorporation of OMMT into SEBS (e.g., SEBS-5) exhibits the highest thermal stability. From the evidence of our previous studies, the thermal stability of SEBS could be obviously improved by addition of high thermally-stable liquid crystalline polymer[43,44] whereas the thermal stability of polyolefinic TPE could not.[45] This leads to the assumption that the significant improvement or reduction in thermal stability of the composite is not only contributed from the inherent nature of nanofiller alone but also the inherent nature of polymer matrix.

To relatively compare the whole kinetic information (E_a, ln$A$, and n) among all samples, Kissinger method determining the kinetic parameters at a fix conversion was employed. Figure 8 presents the Kissinger plots for SEBS, SEBS-5, and OMMT in air. The kinetic parameters (E_a, ln$A$, and n) corresponding to the first stage of degradation for all samples in air are presented in Table II. It is seen that the kinetic parameters change with the composition of the composite. The thermo-oxidative stability of SEBS-5 is significantly improved when compared with that of the neat SEBS. As mentioned earlier, the heat transfer from an external source promotes the formation of charred surface layer of SEBS which combines and intercalates with the resembling silicate layers to provide a sort of ceramic char-layered silicate composite. This carbonaceous silicate structure exhibits as an insulator and mass transport barrier that slows the escape of gaseous products generated during thermal decomposition.[39] Although SEBS-5 become more complex in terms of increasing constituents in the composite compared with the neat SEBS, the decomposition order (n) of SEBS-5 calculated using Kissinger method is lower than that of the matrix polymer. This suggests that the decomposition mechanism becomes less complex with addition of OMMT. The decrease in reaction order of thermal degradation with clay loading associates with the acidic sites (H^+) created on clay layer under heating. It is known that alkylammonium salts in clay galleries can take place with the Hoffmann mechanism leading to volatilization of ammonia and the corresponding olefin.[26,46,47] Therefore, it is believed that the acidic sites in the clay galleries are the key factor for the lowering reaction order of the nanocomposites.[47]

Isothermal decomposition behavior

Isothermal thermogravimetry is complementary and necessary to obtain a concept description of the kinetics of the decomposition process similarly to the nonisothermal one. Figure 9 shows the isothermal TG curves of SEBS, SEBS-5, SEBS-5/5MA, and OMMT at 340°C in air. The corresponding isothermal TG data is presented in Table III. The single-step weight loss and dramatical decomposition of SEBS are observed during the first 30 min of isothermal heating. The similar shape of TG thermograms of SEBS-5 and SEBS-5/5MA with slight difference in actual weight, especially after heating for 40 min, is observed. No significant change in thermal

TABLE II
Nonisothermal Kinetic Parameters for the First Degradation Step in Air of SEBS, SEBS-5, and OMMT Calculated Using Kissinger Method

Sample	E_a (r[a]) (kJ mol^{-1})	n	ln$A$ (min^{-1})
SEBS	93.0 (0.9883)	1.1	16.2
SEBS-5	188 (0.9816)	0.47	30.1
OMMT	156 (0.9350)	0.29	23.8

[a] r means the correlation coefficient for the linear fit analysis.

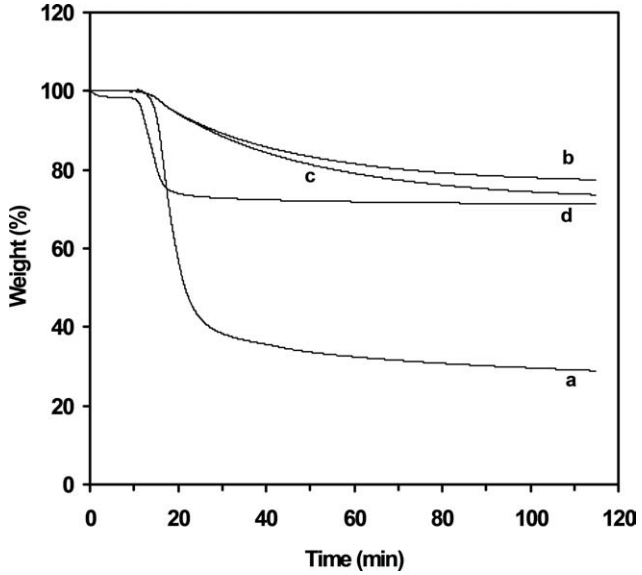

Figure 9 Isothermal TG curves of (a) SEBS, (b) SEBS-5, (c) SEBS-5/5MA, and (d) OMMT under isothermal heating at 340°C in air.

decomposition behavior of SEBS-5 and SEBS-5/5MA is observed which agree well with the results obtained from the nonisothermal measurement as mentioned earlier. This suggests the compatibilizer-independence of thermal stability for this composite system. Interestingly, although the maximum weight loss rate of SEBS and OMMT are relatively high, the composite thereof show a very low maximum weight loss rate. This means that the addition of OMMT into the elastomer matrix significantly inhibit the thermo-oxidative reaction.

Isothermal decomposition kinetics

Effect of isothermal temperatures on thermal decomposition of SEBS, SEBS-5, and OMMT is shown in Figure 10. The shape of the isothermal TG curves strongly depends on the isothermal temperature and composite composition. As seen in Figure 10(a), SEBS exhibits a slow and steady decomposition at 300°C and becomes relatively more rapid with increasing temperature. For SEBS-5 [Fig. 10(b)], a slow and steady decomposition occur at 300, 320, and 340°C. Note that SEBS-5 becomes rapidly degraded with heating at the temperature of 360°C. This indicates that the thermal stability of the composite contributed from the incorporation of OMMT is not pronounced at very high temperature. This means that the addition of OMMT into the elastomer matrix render the retardation of the thermo-oxidative reaction under the isothermal heating in

TABLE III
Thermo-Oxidative Characteristics for the First Degradation Step in Air of SEBS, SEBS-5, SEBS-5/5MA, and OMMT Obtained from Isothermal TG Measurements

Sample	t_{max} (min)	$(d\alpha/dt)_{max}$ (wt % min^{-1})	Char yield (wt %)
SEBS	16.7	9.05	29.6
SEBS-5	16.5	0.94	77.9
SEBS-5/5MA	16.6	0.97	74.4
OMMT	14.6	4.48	71.4

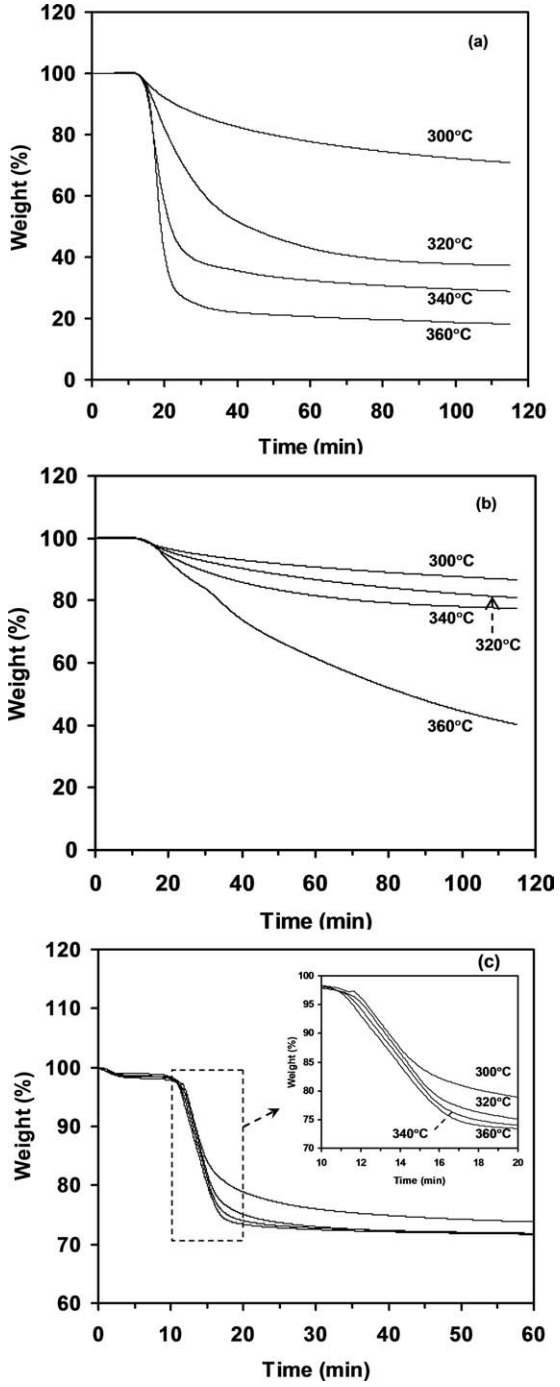

Figure 10 Isothermal TG curves of SEBS (a), SEBS-5 (b), and OMMT (c) under isothermal heating at 300, 320, 340, and 360°C in air.

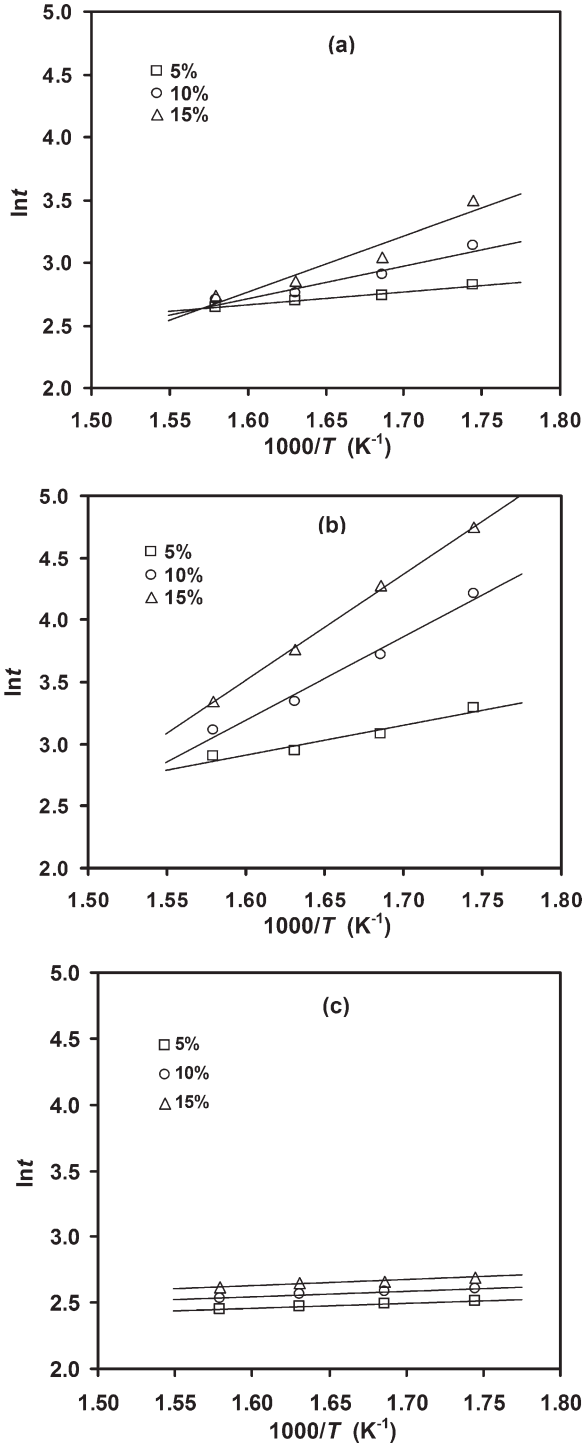

Figure 11 Application of standard isoconversional method to the thermo-oxidative degradation of SEBS (a), SEBS-5 (b), and OMMT (c).

air only up to 340°C. More rapid decomposition with increasing temperature is also observed for OMMT as seen from Figure 10(c).

According to the standard isoconversional method, the plot of ln$t$ versus $1/T$ was investigated to evaluate the E_a value at a particular weight loss. Three straight lines corresponding to particular weight losses of 5, 10, and 15 wt % for SEBS and SEBS-5 and OMMT are illustrated in Figure 11. The respective E_a and ln$A$ values evaluated from the slopes and intercepts of the straight lines for all samples are listed in Table IV. The kinetic parameters (E_a and ln A) of all samples progressively increase with increasing weight loss, indicating that the degradation mechanism varies with the weight loss. The incorporation of OMMT renders an improvement in thermal stability considerably as seen from an increase in E_a value of SEBS-5 when compared with that of the neat SEBS matrix. Note that, the isothermal E_a value of OMMT is relatively lower than that of SEBS, but this nanofiller show a high potential as an enhancing thermal stability component for the elastomeric composite system. The trend of the isothermal results is in agreement with that obtained from the nonisothermal TG data.

To evaluate the order (n) of isothermal degradation, the isoconversional procedure introduced by Friedman[48] was employed. This method is based on taking the natural logarithm of eq. (7) giving

$$\ln\left(\frac{d\alpha}{dt}\right) = \ln A + \ln f(\alpha) - \frac{E_a}{RT} \qquad (10)$$

Term $f(\alpha)$ represents the mathematical expression of the kinetic model. Generally, $f(\alpha)$ is complicated and valid only for limited range of experimental condition. If it is assumed that the degradation reaction is the "simple nth order reaction," $f(\alpha) = (1-\alpha)^n$, eq. (10) can be expressed as

$$\ln\left(\frac{d\alpha}{dt}\right) = \ln A + n\ln(1-\alpha) - \frac{E_a}{RT} \qquad (11)$$

By plotting $\ln(d\alpha/dt)$ against $\ln(1-\alpha)$ at a constant temperature, the isothermal order can be calculated from the slope of the straight line. For instance, the plots of $\ln(d\alpha/dt)$ versus $\ln(1-\alpha)$ for SEBS, SEBS-5 and OMMT at 340°C in air are presented in Figure 12. It is found that the respective n values of SEBS, SEBS-5, and OMMT are found to be 1.1, 4.7, and 0.25. It is seen that the reaction order of SEBS is same as that obtained from nonisothermal data (n = 1.1) whereas the isothermal order of OMMT slightly decreases when compared with the corresponding nonisothermal data. Interestingly, the order of isothermal decomposition for SEBS-5 is much higher than those of SEBS and OMMT, indicating more complex mechanism of OMMT-containing nanocomposite under isothermal heating. Moreover, the thermal degradation of SEBS-5 is more complex under isothermal heating than under dynamic heating as seen from the higher reaction order of isothermal degradation.

TABLE IV
Kinetic Parameters for Isothermal Degradation of SEBS, SEBS-5, and OMMT in Air Calculated by Using Standard Isoconversional Method

Weight loss (%)	E_a[a] (r[b])/ln$A$[a]		
	SEBS	SEBS-5	OMMT
5	8.66 (0.9871)/−0.99	20.2 (0.9379)/1.17	3.21 (0.9967)/−1.91
10	21.8 (0.9416)/1.47	55.9 (0.9831)/7.56	3.36 (0.9883)/−1.89
15	37.4 (0.9229)/4.43	71.3 (0.9988)/10.2	3.74 (0.9845)/−1.84
Average	22.6/1.64	49.1/6.31	3.44/−1.88

[a] The units of E_a and ln$A$ are kJ mol^{-1} and min^{-1}, respectively.
[b] r means the correlation coefficient for the linear fit analysis.

CONCLUSIONS

The thermo-oxidative decomposition of the elastomeric SEBS/OMMT composites was investigated using nonisothermal and isothermal thermogravimetry in air. The nonisothermal TG curve of the OMMT-containing composite shifts to the higher temperature, compared with those of SEBS and OMMT. Similarly, the isothermal TG profile of the nanocomposite shows a slow and steady decomposition whereas more rapid decomposition is observed for SEBS and OMMT. Under dynamic heating and isothermal heating, no significant difference in the thermal stability of the nanocomposites with and without the presence of compatibilizer (SEBS-*g*-MA) is observed. The kinetic parameters (E_a, ln$A$, and n) calculated using the isoconversional method indicates that the incorporation of OMMT into the elastomer matrix significantly improves the thermal stability both under dynamic heating and under isothermal heating. This result has been interpreted by the barrier effect of the OMMT residue on the oxygen flow into the sample. As considered from E_a values, the thermal stability of SEBS, OMMT and their composites is much higher under dynamic heating than isothermal heating. No significant change in the reaction order for SEBS and OMMT under both heating modes, whereas the reaction order of SEBS/OMMT composite is higher under isothermal heating than under dynamic heating, indicating that more complex decomposition process occurs during isothermal degradation.

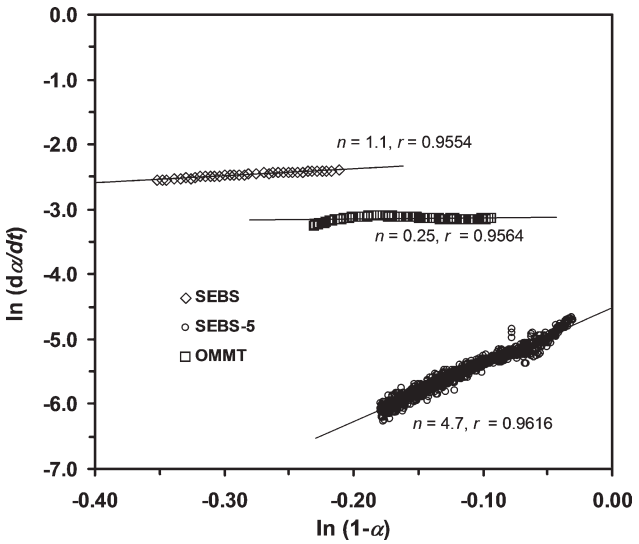

Figure 12 Plots of ln($d\alpha/dt$) versus ln(1 − α) for SEBS, SEBS-5, and OMMT under isothermal heating at 340°C in air (n = isothermal order, r = correlation coefficient for linear fit analysis).

The authors thank Dr. Pornsawan Amornsakchai, Department of Chemistry, Faculty of Science, Naresuan University, for SEM characterization.

References

1. de Paiva, L. B.; Morales, A. R.; Diaz, F. R. V. Appl Clay Sci 2008, 42, 8.
2. Ganguly, A.; De Sarka, M.; Bhowmick, A. K. J Appl Polym Sci 2006, 100, 2040.
3. Lai, S.-M.; Chen, C.-M. Eur Polym J 2007, 43, 2254.
4. Lepoittevin, B.; Devalckenaere, M.; Pantoustier, N.; Alexandre, M.; Kubies, D.; Calberg, C.; Jerome, R.; Henrist, C.; Cloots, R.; Dubois, P. Polymer 2002, 43, 4017.
5. Bao, S. P.; Tjong, S. C. Compos A 2007, 38, 378.
6. Kato, M.; Usuki, A.; Okada A. J Appl Polym Sci 1997, 66, 1781.
7. Osman M. A.; Rupp, J. E. P.; Suter, U. W. Polymer 2005, 46, 1653.
8. Ma, J.; Qi, Z.; Hu, Y. J Appl Polym Sci 2001, 82, 3611.
9. Tjong, S. C.; Bao, S. P.; Liang, G. D. J Polym Sci Polym Phys 2005, 43, 3112.
10. Hotta, S.; Paul, D. R. Polymer 2004, 45, 7639.
11. Li, W.; Huang, Y. D.; Ahmadi, S. J. J Appl Polym Sci 2004, 94, 440.
12. Acharya, H.; Pramanik, M.; Srivastava, S. K.; Bhowmick, A. K. J Appl Polym Sci 2004, 93, 2429.
13. Mohammadpour, Y.; Katbab, A. A. J Appl Polym Sci 2007, 106, 4209.
14. Narr, S. S.; Ramesh, C. Macromolecules 2005, 38, 454.
15. Usuki, A.; Kawasumi, M.; Kojima, Y.; Okada, A.; Kurauchi, T.; Kamigaito, O. J Mater Res 1993, 88, 1174.
16. Liu, X.; Wu, Q.; Zhang, Q.; Mo, Z. J Polym Sci Polym Phys 2002, 41, 63.
17. Chen, G. X.; Yoon, J. S. J Polym Sci Polym Phys 2005, 43, 817.
18. Ou, C. F.; Ho, M. T.; Lin, J. R. J Polym Res 2003, 10, 127.
19. Ke, Y.; Long, C.; Qi, Z. J Appl Polym Sci 1999, 71, 1139.

20. Lao, M.; Zhu, J.; Xu, H.; Li, Y.; Shan, W. J Appl Polym Sci 2004, 92, 3430.
21. Chang, Y.-W.; Shin, J.-Y.; Ryu, S. H. Polym Int 2004, 53, 1047.
22. Lim, S. T.; Lee, C. H.; Kwon, Y. K.; Choi, H. J. J Macromol Sci Phys 2004, 43B, 577.
23. Lee, C. H.; Kim, H. B.; Lim, S. T.; Kim, H. S.; Kwon, Y. K.; Choi, H. J Macromol Chem Phys 2006, 207, 444.
24. Legg, N. R.; Holden, D.; Schroder, H. E., Eds. Thermoplastic Elastomers; Hanser: Munich, 1987.
25. Marazzato, C.; Peneva, Y.; Lefterova, E.; Filippi, S.; Minkova, L. Polym Test 2007, 26, 526.
26. Qin, H.; Zhang, S.; Zhoa, C.; Yang, M. J Polym Sci B Polym Phys 2005, 43, 3713.
27. Ozawa, T. Bull Chem Soc Jpn 1965, 38, 1881.
28. Flynn, J. H.; Wall, L. A. J Res Natl Bur Stds 1966, 70A, 487.
29. Kissinger, H. E. Anal Chem 1957, 29, 1702.
30. Tanaka, H. Thermochim Acta 1995, 267, 29.
31. Nam, J. D.; Seferis, J. C. J Polym Sci B Polym Phys 1991, 29, 601.
32. Vyazovkin, S.; Wight, C. A. J Phys Chem 1997, 101, 8279.
33. Roduit, B.; Maciejewski, M.; Baiker, A. Thermochim Acta 1996, 282/283, 101.
34. Le Bras, M.; Rose, N.; Burbigot, S.; Henry, Y.; Delobel, R. J Fire Sci 1996, 37, 173.
35. Vyazovkin, S. Thermochim Acta 2000, 355, 155.
36. Vaia, R. A.; Giannelis E. P. Macromolecules 1997, 30, 8000.
37. Filipi, S.; Yordanov, H.; Minkova, L.; Polacco, G.; Talarico M. Macromol Mater Eng 2004, 289, 512.
38. Allen, N. S.; Edge, M.; Wilkinson, A.; Liauw, C. M.; Mouretou, D.; Barrio, J.; Martinez-Zaporta, A. Polym Degrad Stabil 2001, 71, 113.
39. Zanetti, M.; Bracco, P.; Costa, L. Polym Degrad Stabil 2004, 85, 657.
40. Saikrasun, S.; Saengsuwan, S. J Mater Proc Technol 2009, 209, 3490.
41. Hatakeyama, T.; Quinn, F. X. Thermal Analysis: Fundamentals and Applications to Polymer Science, 2nd ed.; Wiley: Chichester, 1999.
42. Peterson, J. D.; Vyazovkin, S.; Wight, C. A. Macromol Chem Phys 2001, 202, 775.
43. Saikrasun, S.; Amornsakchai, T. J Appl Polym Sci 2006, 101, 1610.
44. Saikrasun, S.; Amornsakchai, T. J Elast Plast 2007, 39, 213.
45. Saikrasun, S.; Amornsakchai, T. J Appl Polym Sci 2008, 107, 2375.
46. Qin, H. L.; Zhang, Z. G.; Feng, M.; Gong, F. L.; Zhang, S. M.; Yang, M. S. J Polym Sci B Polym Phys 2004, 42, 3006.
47. Zanetti, M.; Camino, G.; Reichert, P.; Mulhaupt, R. Macromol Rapid Commun 2001, 22, 166.
48. Friedman, H. J Polym Sci C Polym Symp 1964, 6, 183.